



OPEN ACCESS

EDITED BY

Weimin Shen,
Children's Hospital of Nanjing Medical
University, China

REVIEWED BY

Birsen Karaman,
Istanbul University, Türkiye
Xuanye Cao,
University of Texas MD Anderson Cancer
Center, United States

*CORRESPONDENCE

Xiaojun Tang
✉ frog30@126.com

SPECIALTY SECTION

This article was submitted to Pediatric
Orthopedics, a section of the journal *Frontiers
in Pediatrics*

RECEIVED 16 November 2022

ACCEPTED 24 January 2023

PUBLISHED 13 February 2023

CITATION

Liu B, Liu W, Zhao S, Ma L, Zang T, Huang C,
Shu K, Gao H and Tang X (2023) Transcriptome
sequencing of facial adipose tissue reveals
alterations in mRNAs of hemifacial microsomia.
Front. Pediatr. 11:1099841.
doi: 10.3389/fped.2023.1099841

COPYRIGHT

© 2023 Liu, Liu, Zhao, Ma, Zang, Huang, Shu,
Gao and Tang. This is an open-access article
distributed under the terms of the [Creative
Commons Attribution License \(CC BY\)](#). The use,
distribution or reproduction in other forums is
permitted, provided the original author(s) and
the copyright owner(s) are credited and that the
original publication in this journal is cited, in
accordance with accepted academic practice.
No use, distribution or reproduction is
permitted which does not comply with these
terms.

Transcriptome sequencing of facial adipose tissue reveals alterations in mRNAs of hemifacial microsomia

Bingyang Liu¹, Wei Liu¹, Shanbaga Zhao¹, Lunkun Ma¹, Tianying Zang¹,
Changjin Huang¹, Kaiyi Shu¹, Hengbin Gao² and Xiaojun Tang^{1*}

¹Department of Craniomaxillofacial Surgery, Plastic Surgery Hospital, Chinese Academy of Medical Sciences and Peking Union Medical College, Beijing, China, ²State Key Laboratory of Crop Biology, College of Life Sciences, Shandong Agricultural University, Tai'an, China

Hemifacial microsomia (HFM) is a common congenital malformation of the craniofacial region, including mandibular hypoplasia, microtia, facial palsy and soft tissue deficiencies. However, it remains unclear which specific genes are involved in the pathogenesis of HFM. By identifying differentially expressed genes (DEGs) in deficient facial adipose tissue from HFM patients, we hope to provide a new insight into disease mechanisms from the transcriptome perspective. RNA sequencing (RNA-Seq) was performed with 10 facial adipose tissues from patients of HFM and healthy controls. Differentially expressed genes in HFM were validated by quantitative real-time PCR (qPCR). Functional annotations of the DEGs were analyzed with DESeq2 R package (1.20.0). A total of 1,244 genes were identified as DEGs between HFM patients and matched controls. Bioinformatic analysis predicted that the increased expression of *HOXB2* and *HAND2* were associated with facial deformity of HFM. Knockdown and overexpression of *HOXB2* were achieved with lentiviral vectors. Cell proliferation, migration, and invasion assay was performed with adipose-derived stem cells (ADSC) to confirm the phenotype of *HOXB2*. We also found that PI3K–Akt signaling pathway and human papillomavirus infection were activated in HFM. In conclusion, we discovered potential genes, pathways and networks in HFM facial adipose tissue, which contributes to a better understanding of the pathogenesis of HFM.

KEYWORDS

hemifacial microsomia, *HAND2*, *HOXB2*, facial adipose tissue, RNA sequencing

Introduction

Hemifacial microsomia (HFM) is one of the most common congenital craniofacial defects, incidence of which ranges from 1:13,500 to 1:5,600 (1), second only to cleft lip and palate. HFM, which was first described in 1,881 (OMIM *164210), typically affects the external ear, middle ear, mandible and temporomandibular joint, mastication and facial muscles, and other facial soft tissues on the affected side. In some affected patients, anomalies may also include in cardiac, vertebral, and central nervous system in addition to craniofacial anomalies. They significantly affect facial appearance and physiological function, posing a substantial psychological and financial burden on families.

The precise etiology and physiopathology of HFM are far from being completely understood and both environmental and genetic factors can be considered to interpret the symptoms of HFM. In terms of environmental factors, the embryo is vulnerable to teratogens, such as thalidomide (2), retinoic acid (3), vasoactive medications, and alcohol (4), which may result in permanent congenital malformations, including HFM. In addition, maternal diabetes (5), multiple gestations, and vaginal bleeding during pregnancy (4) are also major risk factors for HFM. Despite the fact that most cases of HFM are sporadic, familial occurrence suggests a

genetic predisposition. Most cases of familial occurrence show an autosomal dominant transmission, which accounts for 2% to 10% of cases (6). Currently, most studies on HFM are limited to evaluating one or more genes for expression alterations, but systematic research on differentially expressed genes or primary pathways is lacking. As a result, HFM is an enigmatic condition with an unknown etiology and poorly understood pathogenesis. It is essential to understand how disease develops and pathogenesis occurs by interpreting transcriptomes. Reports have not been found about the global transcriptome abnormalities of the facial adipose tissue from patients with HFM. Next-generation sequencing (NGS) is well-established for deciphering the transcriptome using high-throughput and quantitative methods (7). The aim of our study is to identify differentially expressed genes (DEGs) and molecular pathways in facial adipose tissue from patients with HFM, which will provide new insights into disease mechanisms at the molecular level.

Materials and methods

Patients and clinical samples

Patients were diagnosed and recruited based on typical clinical symptoms of mandibular, ear and facial soft tissue hypoplasia, physical examination results, and imaging reports including x-ray and CT reports. All samples were collected from Department of maxillofacial surgery, Plastic Surgery Hospital, Chinese Academy of Medical Sciences, Peking Union Medical College. All participants enrolled in our present study were Han Chinese, Asia population.

Six patients with HFM and four healthy controls were enrolled in our study. All patients' adipose tissue samples in our manuscript were collected through scar excision when removing the mandibular distractor surgery. The adipose tissue from controls was also collected through the buccal fat pad resection procedure from patients with facial fat accumulation. After taking adipose tissue away from operating table, we dissected it into small pieces with surgical scissors. Samples were maintained in centrifuge tubes with RNAlater (Ambion Inc) and stored at -80°C as the first part, preserved in cryotub.

According to the Declaration of Helsinki Principles, the protocols for the study were approved by the Ethics Review Committee of Plastic Surgery Hospital. Written informed consent was obtained from participants.

RNA sequencing (RNA-seq)

According to the manufacturer's instructions, total RNA was isolated from adipose tissues using the RNeasy Lipid Tissue Mini Kit (QIAGEN). In accordance with the manufacturer's instructions, stranded total RNA LT sample prep kit (Illumina) was used to prepare the compatible library. A Bioanalyzer (Agilent) was used to analyze the quality and concentration of all libraries. Sequencing of mRNA was performed on an Illumina HiSeq 2,500 sequencing system (Illumina), and 150-bp paired-end FASTQ files were generated.

cDNA preparation and quantitative PCR

Total RNA was isolated with the TRIzol reagent (Thermo Fisher Scientific) according to the manufacturer's protocol. The RNA concentration and purity were evaluated with NanoDrop ND-2000 spectrophotometer (Thermo Fisher Scientific Inc). With $1\ \mu\text{g}$ of RNA in the $20\ \mu\text{l}$ reaction system, reverse transcription reactions were performed with PrimeScript Reverse Transcriptase (Takara Bio) according to the manufacturer's instructions.

To validate the confidence of RNA-Seq, several differentially expressed genes were selected and analysed by quantitative real-time PCR (qPCR) utilizing the SYBR Premix EX Taq reagent (Takara) in a QuantStudio 7 Flex Real-Time PCR System (Applied Biosystems). Primers (Supplementary Table S1) were designed for the coding sequences of the candidate genes in Primer 3 software (<http://frodo.wi.mit.edu/cgi-bin/primer3>). GAPDH was used as the internal control. qPCR replicates were performed in a final volume of $10\ \mu\text{l}$ containing primers, SYBR Premix EX Taq reagent (Takara) and cDNA templates. All quantitative PCRs were performed for three biological replicates. The relative expression levels of the candidate genes were calculated as the averaged normalized Ct value of each sample compared with the GAPDH Ct value of the corresponding sample based on the $2^{-\Delta\Delta\text{Ct}}$ method.

Detection of differentially expressed genes

Our RNA expression levels were estimated using HISAT2 (version 2.1.0). Genome sequence data (hg19, Genome Reference Consortium GRCh37) and annotation data were obtained from UCSC website (<https://genome.ucsc.edu>). With featureCounts (v1.5.0-p3), we calculated transcript counts at the gene level and relative abundances in FPKM (fragments per kilobase of exon per million fragments mapped). We build Principal Component Analysis (PCA) and identified 1,234 differential expressed genes (DEGs) by using DESeq2 (P -value <0.05 , $\log_2\text{Foldchange} >2$) (8). Heatmap show the gene expression pattern in different groups, all DEGs expression level were scale to -2 and 2 based on Z-score calculation. Diagrams were visualized by ggplot2 in R version 4.1.0.

Gene annotation: gene ontology and pathway analysis

The KEGG (Kyoto Encyclopedia of Genes and Genomes database) and gene ontology (GO) pathway enrichment analysis was performed using ClusterProfiler package from BioConductor (<http://www.bioconductor.org/>). A hypergeometric exact test was used to classify enrichment GO categories and KEGG pathways. Only terms with a P -value 0.05 were considered enriched. According to the rank of P -value, we display the top 20 GO enriched terms for both upregulated and downregulated genes.

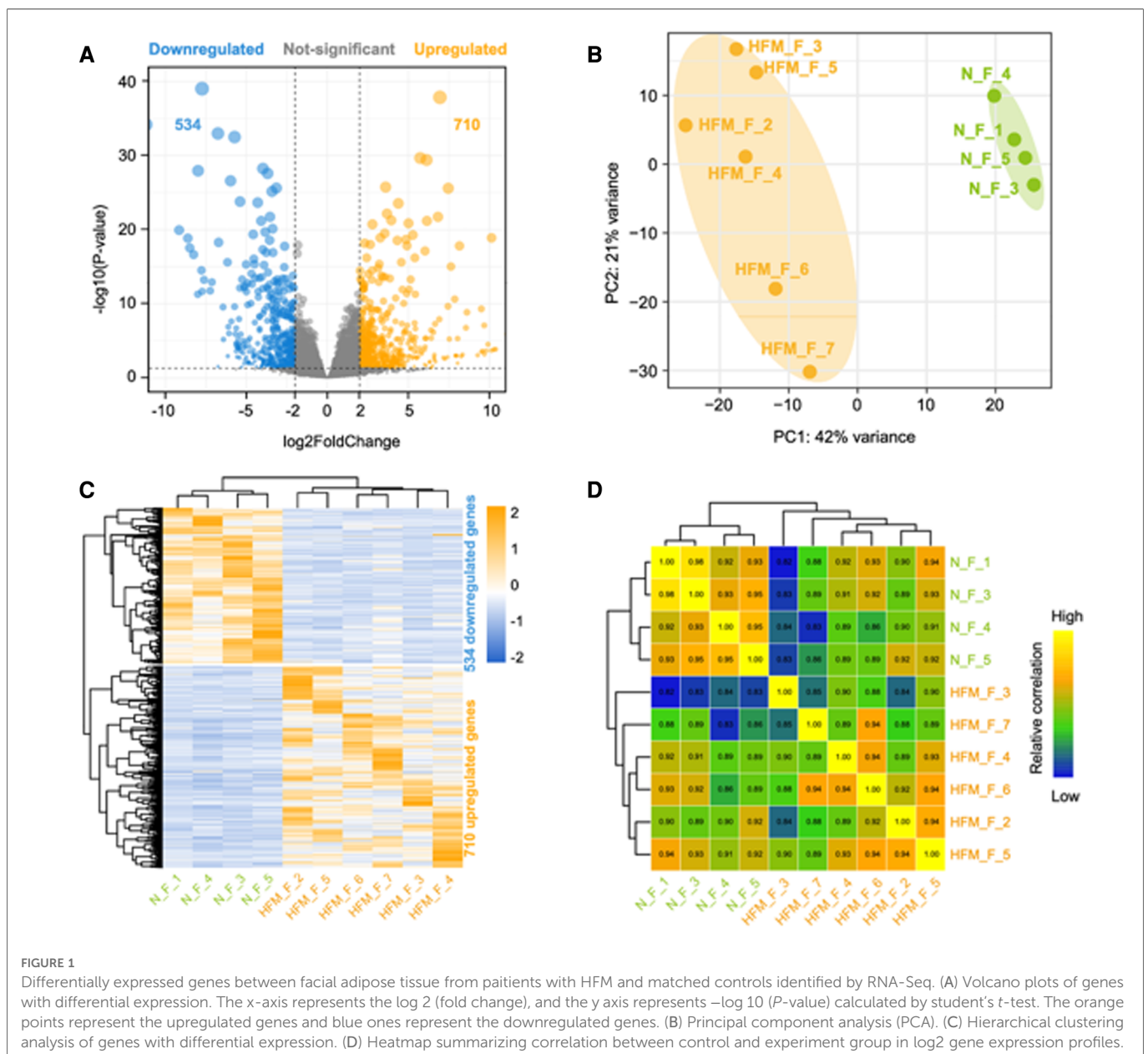
Cell lines, transfection and construction of lentiviral vectors

The buccal fat pad from healthy controls were collected in D-Hanks solution with 1,000 U/L penicillin streptomycin (Solarbio, Beijing, China). An equal volume of 0.25% of EDTA trypsin supplemented with 0.1% of type I collagenase solution was added, and the samples were gently vibrated in a 37°C incubator shaker for 45 min. Cells were collected and centrifuged at 1,000 rpm for 10 min; the supernatant was removed, and the cells were resuspended with DMEM supplemented with 10% FBS. After filtering using a 100-mesh sieve, cells were transferred into a culture dish and incubated in 37°C with 5% CO₂ for 24 h. Cells were observed using a phase-contrast microscope daily. Cell morphology and proliferating rates were recorded, and when cells reached 90%–95% confluence, cells were digested with 0.25% EDTA trypsin and subcultured into several culture dishes. Lentiviral interference

vectors, pCMV.GFP&PR.U6 (sh-, interference vector), and lentiviral overexpression vector, VP001-CMV-MS-3flag-EF1-ZsGreen-T2A-PURO (oe-, overexpression vector), were purchased from Sangon Biotech (Shanghai, China) and General Biosystems (Anhui,China). A lentiviral-based *HOXB2* interference vector, a *HOXB2* overexpression vector were constructed. Lentiviral infections were performed using protocols available online (www.broadinstitute.org). Next, cells were inoculated into a six-well plate at a density of 5×10^4 cells/ml and infected with NC, si-*HOXB2*, vector, *HOXB2*-OE, respectively.

Cell proliferation, transwell assays

For the cell proliferation test, a CCK8 Kit (Solarbio, China) was used. In 96-well plates, cells were seeded in 96-well flat-bottomed plates with each well containing 2,000 cells in 200 μ l of culture medium and cultured in ambient environment described above.



CCK8 reagent was added into wells, after incubation at 37°C for 24 h in a humidified incubator with 5% CO₂, the proliferative ability of the cells was measured at 450 nm. For transwell migration assay, different cells were suspended in 200 μ l of DMEM without FBS and seeded on the top chamber of 24-well plate-sized Transwell inserts (Corning Falcon). The lower chambers contained DMEM with 20% FBS. After incubation for 8 h, the inserts were fixed and stained with crystal violet. Cells in the upper chamber were removed with cotton swabs. The average confluence of migrated cells was analyzed by ImageJ according to three random fields captured by 100 \times microscope. Each experiment was conducted in triplicate.

Result

Clinical characteristics in the HFM and healthy control groups

The 6 patients with HFM enrolled in our study who were aged from 7 to 26. All patients were classified with Pruzansky II and III

mandibular hypoplasia, including facial soft tissue deficiencies, shortened mandibular ramus, small glenoid fossa, malformed condyle, preauricular tags, microtia, excluding other concurrent clinical symptoms (epibulbar dermoids and vertebral anomalies). The 4 matched controls were all adults who aged from 20 to 25. The adipose tissue was collected when matched controls underwent buccal fat pad resection. The clinical details of the participants are provided in [Supplementary Table S2](#).

RNA-seq analysis and identification of differentially expressed genes

A transcriptomic analysis of adipose tissue from six patients with HFM and four healthy control was conducted to better understand the pathogenesis of the disease. A total of 28 million read pairs were obtained from each sample and were compared between the HFM and control groups in adipose tissue. The total number of annotated mRNAs identified was 333,341 and 1,244 mRNAs were significantly deregulated (q -value $< .05$; absolute value Log_2 Ratio ≥ 1)

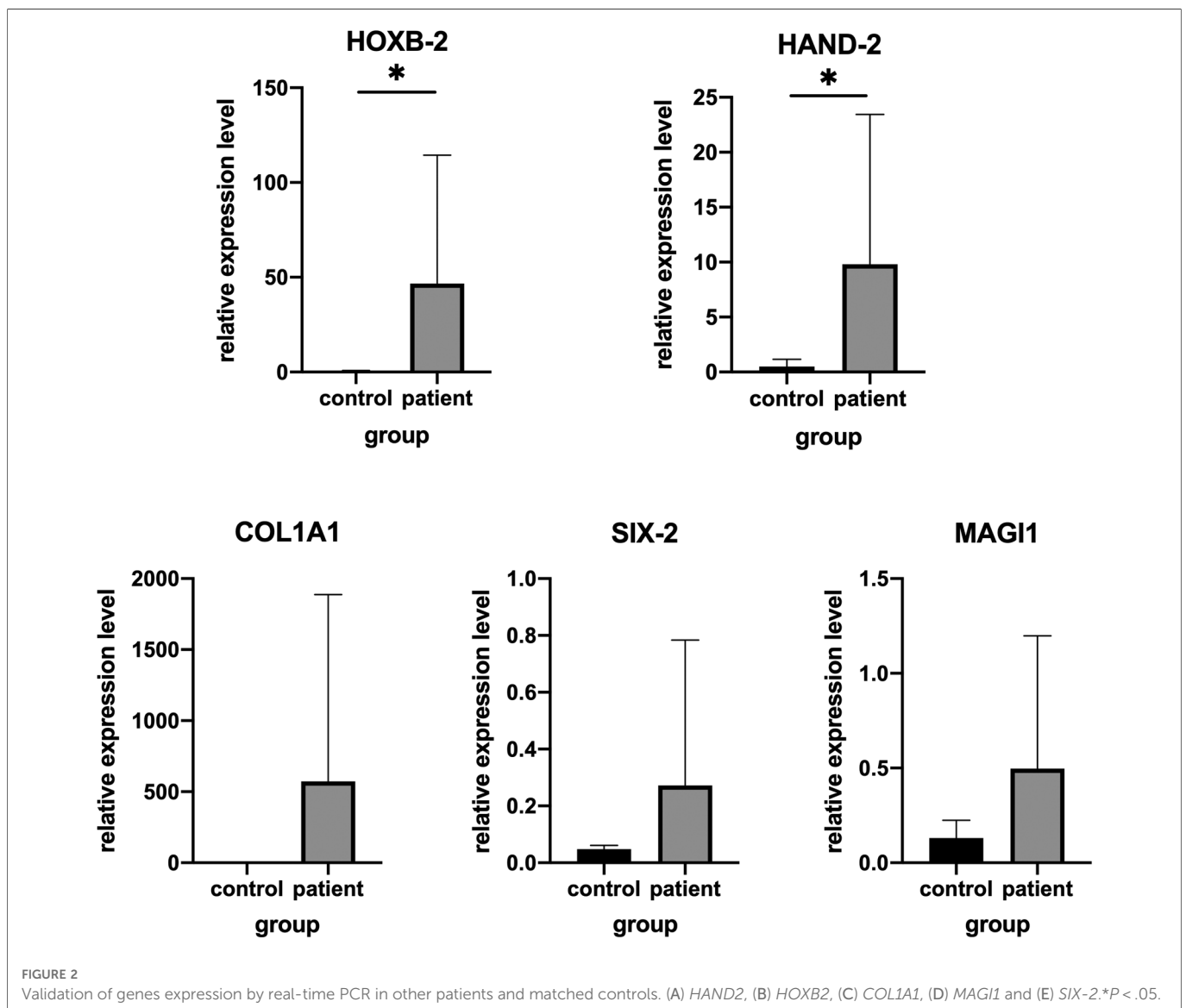
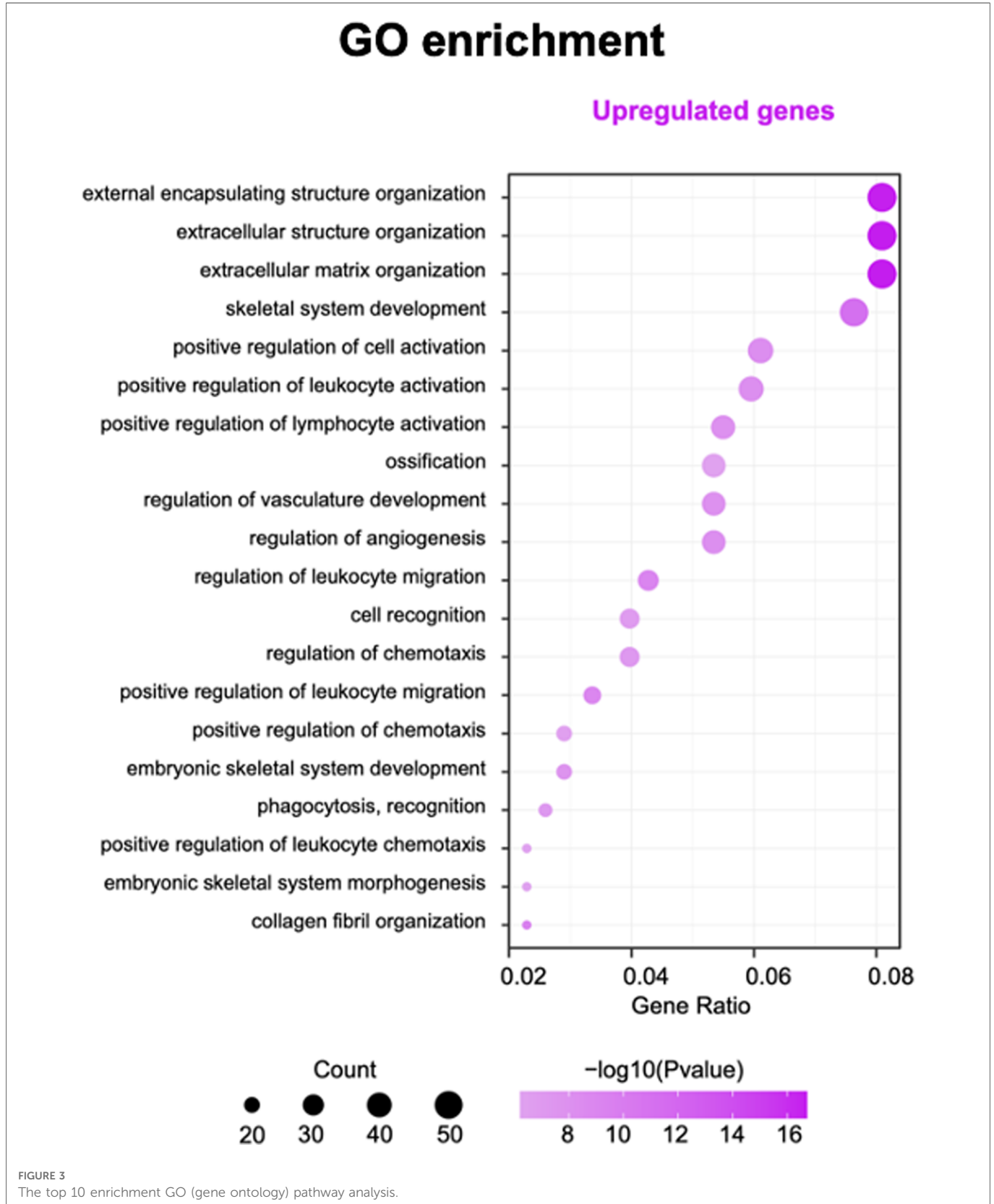


(Figure 1A). A comparison of the adipose tissues from patients with HFM and those from controls demonstrated that 710 genes were up-regulated, and 534 genes were down-regulated. The differentially expressed mRNA data sets were analyzed using principal component

analysis and hierarchical clustering. HFM adipose tissue exhibited distinct gene expression profiles compared with control adipose tissue based on PCA (Figure 1B). According to a hierarchical clustering analysis of the differentially expressed genes in adipose



tissue from patients with HFM and control subjects, each gene expression pattern clustered separately (Figure 1C). Subsequently, we draw a correlation heatmap between various gene expression (Figure 1D). The results indicated that HFM has a profound impact on the expression of mRNA in the facial adipose tissue.

Validation of mRNA expression

To confirm the accuracy of RNA-Seq, five genes including up-regulated (*HOXB2*, *HAND2*, *COL1A1*, *MACH1*) and down-regulated (*SIX2*) between adipose tissue from patient with HFM and controls were selected for further validation in additional set of clinical samples. Consistent with our expectation, the validation results of *HOXB2* and *HAND2* were consistent with the RNASeq data. While no significant difference ($P > 0.05$) was detected in the levels of *COL1A1*, *MACH1*, *SIX2* mRNA, according to the results of quantitative real-time PCR (Figure 2).

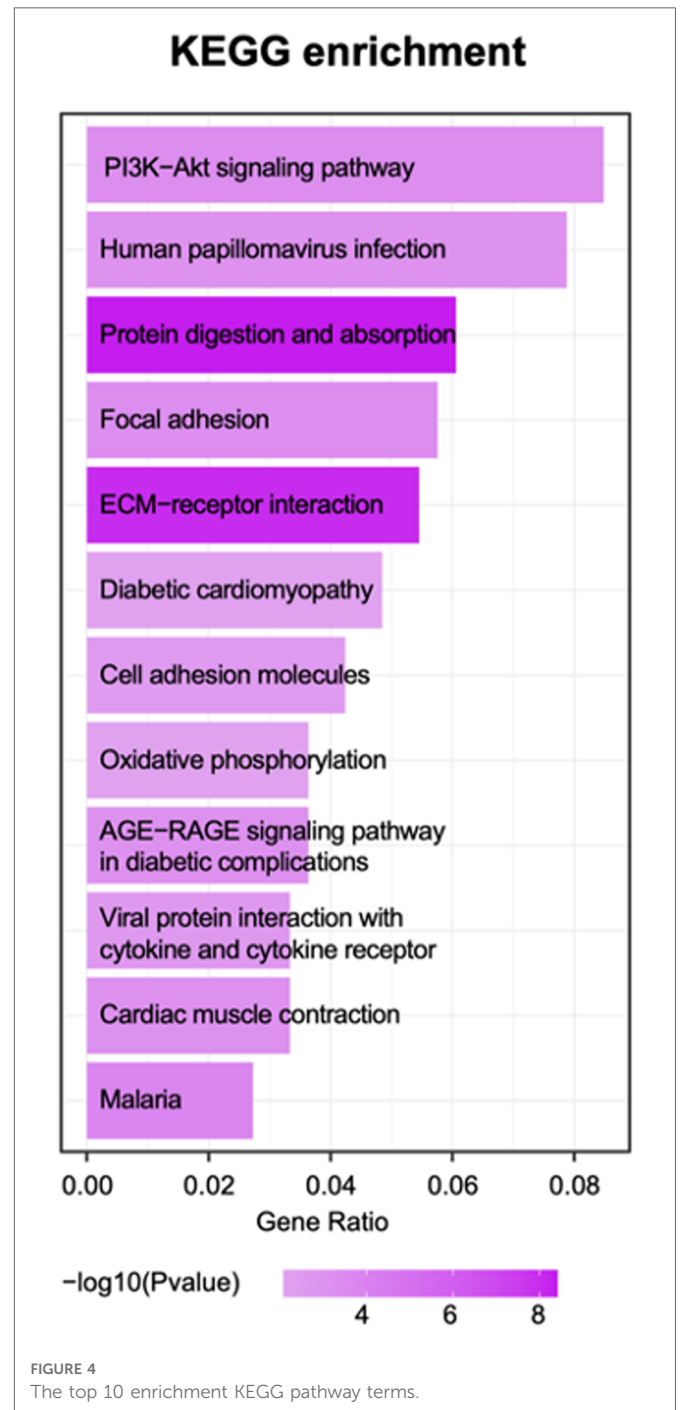
Functional analysis of differentially expressed genes

Gene ontology and pathway analysis of genes were performed to find possible biological alterations related to HFM. A wide range of biological functions and signaling pathways are involved with DEGs. The immune system and the skeletal system exhibited the most significant differences, out of many involved pathways.

Based on the enrichment score, we selected the top ten items from GO (Figure 2). the most significant biological processes related to craniofacial morphogenesis included skeletal system development, ossification, regulation of vasculature development, embryonic skeletal system development and embryonic skeletal system morphogenesis. According to KEGG analysis (Figure 3), signal pathways including PI3K–Akt signaling pathway and Human papillomavirus infection showed significant differences. The PI3K–Akt signaling pathway was previously shown to be associated with NCCs development (9). The relationship between human papillomavirus infection and HFM has not been reported yet. Additional studies are required to further investigate these possibilities.

Effect of *HOXB2* on ADSC

To examine the effects of *HOXB2* on ADSC proliferation and metastasis, we conducted a series of cell function experiments. *HOXB2* overexpression significantly decreased the migration and invasion of ADSC (Figures 4A–D), as well as reduced their proliferation (Supplementary Additional file S1, Figure S2B). On the contrary, Loss of *HAND2* further enhanced cell migration and invasion of these ADSC (Supplementary Additional file S1, Figure S2F, S3B–D).



Discussion

The molecular mechanism underlying HFM remains unclear. Numerous studies revealed that HFM has multiple contributors, including genetic, maternal, and environmental factors (10). Three main hypotheses have been suggested to explain the pathogenesis of HFM: stapedia artery abnormalities, abnormal development of cranial neural crest cells (CNCCs), and injury of Meckel's cartilage. In this study, RNA-Seq has been used for the first time to analyze the transcriptome of affected facial adipose tissue of HFM in Han Chinese.

CNCCs are highly capable of proliferating and diffusing during the embryonic period, which plays a vital role in the growth and

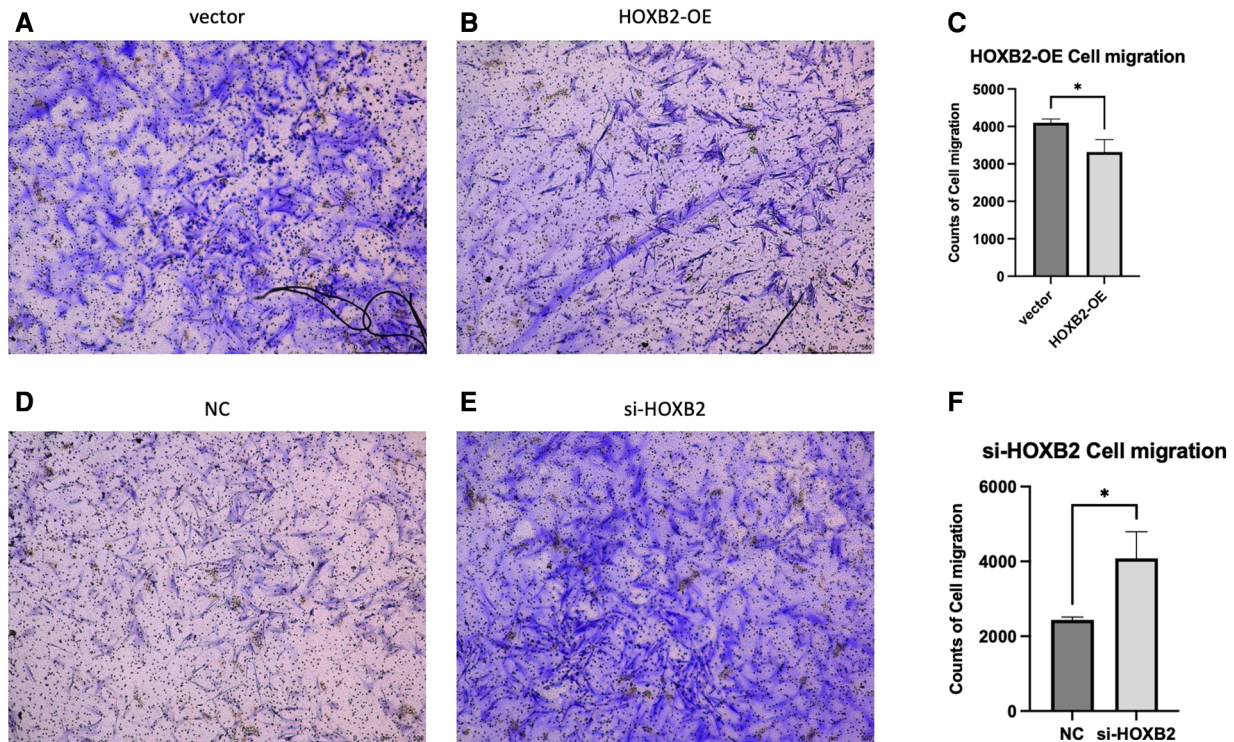


FIGURE 5 (A–C) overexpression of *HOXB2* inhibited ADSC migration. (D–F) Knockdown of *HOXB2* expression have enhanced ADSC migratory ability.

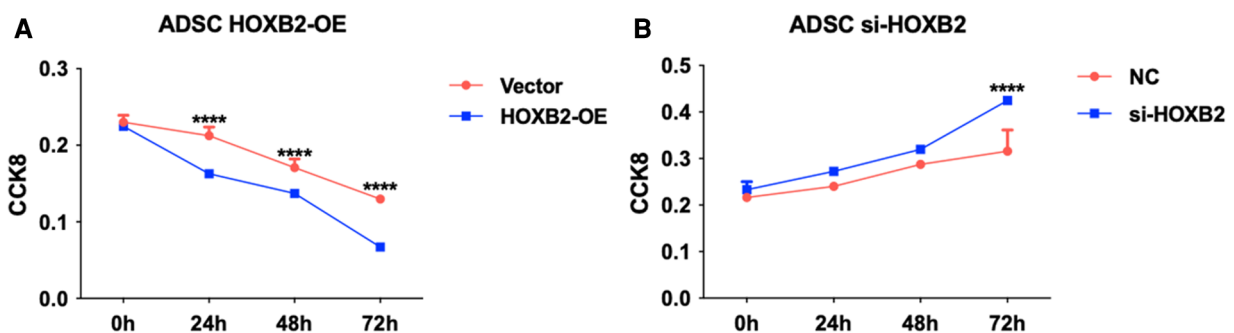


FIGURE 6 (A) *HOXB2* overexpression inhibited ADSC proliferation. (B) *HOXB2* knockdown increased the ADSC proliferation ability.

development of craniofacial cartilage, bone tissue, as well as smooth muscle, sensory nerve, and adipose tissues (11). One-third of all congenital anomalies are related to improper development of neural crest cells (NCCs) in humans (12). The majority of abnormal craniofacial tissue involved in HFM is derivatives of CNCCs. Different parts of CNCCs have specific migration paths, forming the first and second branchial arches. Thus, it is a possible mechanism of HFM that affects the proliferation, migration, and differentiation of CNCCs (10).

To our knowledge, this is the first study using Next-generation sequencing to compare the differential expression of genomic profiles between HFM patients' and healthy controls' facial adipose tissue. Our results indicated that overexpressed of *HAND2* and *HOXB2* may resulted in the alteration of hemifacial hypoplasia in HFM patients.

HAND2 (Heart And Neural Crest Derivatives Expressed 2) is a protein coding gene which plays an important role in limb and branchial arch development (13). *HAND2* expression in the ventral region of the branchial arch is independent of Edn1/Ednra-mediated signals (14). The expression of *HAND2* in wild type embryos is restricted to the distal mandibular mesenchyme, which is downstream of Bmp4 (15, 16). Studies indicated that overdosed BMP signaling inhibits facial skeletal formation by causing dramatic apoptosis in NCC cells (17).

According to research, high *HAND2* expression in NCCs can result in the transformation of the upper jaw into a lower jaw, resulting in the absence of a secondary palate (18). Funato et al. experiments have indicated *HAND2*-overexpressed mice showed fragmented temporal bones and malformed middle ear (malleus,

incus, gonial bone, and tympanic ring) (18). *HAND2* overexpression caused hypoplastic bone formation in the cranial region, consistent with the observation that *HAND2* negatively affects mandibular ossification through direct inhibition of *RUNX2*, a master transcription factor of osteoblast-specific genes (19). These experimental results are consistent with the observed clinical manifestations in HFM patients including underdevelopment of the mandible, maxilla, ear, orbit, facial soft tissue.

HOX genes, which encode for homeodomain-containing transcription factors, are major inhibitors involved in patterning of animal embryos and craniofacial program carried by CNCC (20, 21). *HOXA2*, as other *HOX2* paralogs, may cooperate with *HOXB2* in the second pharyngeal arch (22). A prevalent role of *HOXA2* as its inactivation in mouse induced a mirror-image duplication of the lower jaw with two Meckel's cartilage (23, 24). Studies have also shown that patients with mutations in *HOXA2* display severe microtia, middle ear deformities and hearing loss (25, 26). In Animal experiments, the hearing impairment were also observed in *HOXB2* mutants (27). On the other HAND, *HOXA2* homozygous mutant embryos contained additional, more extensive ossification centers (23). Histological observations of *HOXB2* mutant mice detected a cartilage rod carrying a proximal protuberance, which could be interpreted as a triplicated malleus (28). Apart from triplicated malleus, the *HOXA2* mutants duplicate all skeletal elements normally derived from the first arch NCC, including ectopic Meckel's cartilage, as well as ectopic incus, malleus, tympanic, and squamous bones (24). In our experiments, it can be observed that high expression of *HOXB2* can significantly reduce ADSC migration and proliferation. Unfortunately, no animal experiments about overexpression of *HOXB2* can be found in the literature. Further verification experiments will be conducted in order to confirm the gene function. We could only speculate the overexpression of *HOXB2* were possibly in accordance with the clinical symptoms in HFM.

For the first time, we identified two mRNAs that may participate in the pathogenesis of HFM, providing a new avenue for future research. Suppressing the expression of genes, such as *HOXB2* and *HAND2*, might be a promising therapeutic approach to HFM. However, there are several limitations in our study. First of all, the sample size is small, and more samples will be collected for further study. In addition, we have not provided experimental evidence to support the role of genes. Furthermore, as the samples were collected with a wide range of ages, a comparison of HFM samples to normal adipose tissue may reveal different genes due to the tissues' developmental stages but not because of differences between them. In summary, it is necessary to further explore the underlying roles of the identified pathways and molecules in HFM.

Conclusion

As a result, we identified 1,275 DEGs in adipose tissue of HFM patients along with key pathways and networks. It is the first study to report that HFM is related to high expression of *HAND2* and *HOXB2*, providing an important basis for further mechanistic investigations of HFM. A detailed study of these two genes in HFM pathogenesis will be conducted in the near future.

Data availability statement

The datasets presented in this study can be found in online repositories. The names of the repository/repositories and accession number(s) can be found below: <https://ngdc.cncb.ac.cn/gsa-human/s/QUhld0aT,HRA002742>.

Ethics statement

The studies involving human participants were reviewed and approved by Ethics Review Committee of Plastic Surgery Hospital. Written informed consent to participate in this study was provided by the participants' legal guardian/next of kin.

Author contributions

SZ and LM: Conceptualization, Methodology. CH and TZ: Data curation, Writing- Original draft preparation. KS: Visualization, Investigation. XT: Supervision. BL: Writing- Reviewing and Editing, WL: Surgical instruction, Specimen taking. HG: Bioinformatics analysis. All authors contributed to the article and approved the submitted version.

Funding

CAMS Innovation Fund for Medical Sciences (2021-I2M-1-068) the Special Research Fund for Plastic Surgery Hospital, Chinese Academy of Medical Sciences and Peking Union Medical College Nos. (YS202009).

Conflict of interest

The authors declare that the research was conducted in the absence of any commercial or financial relationships that could be construed as a potential conflict of interest.

Publisher's note

All claims expressed in this article are solely those of the authors and do not necessarily represent those of their affiliated organizations, or those of the publisher, the editors and the reviewers. Any product that may be evaluated in this article, or claim that may be made by its manufacturer, is not guaranteed or endorsed by the publisher.

Supplementary material

The Supplementary Material for this article can be found online at: <https://www.frontiersin.org/articles/10.3389/fped.2023.1099841/full#supplementary-material>.

References

- Hartsfield JK. Review of the etiologic heterogeneity of the oculo-auriculo-vertebral spectrum (Hemifacial Microsomia). *Orthod Craniofac Res.* (2007) 10:121–8. doi: 10.1111/j.1601-6343.2007.00391.x
- Poswillo D. The pathogenesis of the first and second branchial arch syndrome. *Oral Surg Oral Med Oral Pathol.* (1973) 35:302–28. doi: 10.1016/0030-4220(73)90070-4
- Mondal D, Shenoy RS, Mishra S. Retinoic acid embryopathy. *Int J Appl Basic Med Res.* (2017) 7:264–5. doi: 10.4103/ijabmr.IJABMR_469_16
- Werler MM, Starr JR, Cloonan YK, Speltz ML. Hemifacial microsomia: from gestation to childhood. *J Craniofac Surg.* (2009) 20(Suppl 1):664–9. doi: 10.1097/SCS.0b013e318193d5d5
- Wang R, Martínez-Frías ML, Graham JM Jr. Infants of diabetic mothers are at increased risk for the oculo-auriculo-vertebral sequence: a case-based and case-control approach. *J Pediatr.* (2002) 141:611–7. doi: 10.1067/mpd.2002.128891
- Ballesta-Martínez MJ, López-González V, Dulcet LA, Rodríguez-Santiago B, García-Miñaur S, Guillen-Navarro E. Autosomal dominant oculoauriculovertbral spectrum and 14q23.1 microduplication. *Am J Med Genet A.* (2013) 161a:2030–5. doi: 10.1002/ajmg.a.36007
- Wang Z, Gerstein M, Snyder M. RNA-Seq: a revolutionary tool for transcriptomics. *Nat Rev Genet.* (2009) 10:57–63. doi: 10.1038/nrg2484
- Love MI, Huber W, Anders S. Moderated estimation of fold change and dispersion for RNA-seq data with DESeq2. *Genome Biol.* (2014) 15:550. doi: 10.1186/s13059-014-0550-8
- Geary L, LaBonne C. FGF Mediated MAPK and PI3K/Akt Signals make distinct contributions to pluripotency and the establishment of Neural Crest. *Elife.* (2018) 7. doi: 10.7554/eLife.33845
- Beleza-Meireles A, Clayton-Smith J, Saraiva JM, Tassabehji M. Oculo-auriculo-vertebral spectrum: a review of the literature and genetic update. *J Med Genet.* (2014) 51:635–45. doi: 10.1136/jmedgenet-2014-102476
- Mehrotra P, Tseropoulos G, Bronner ME, Andreadis ST. Adult tissue-derived neural crest-like stem cells: sources, regulatory networks, and translational potential. *Stem Cells Transl Med.* (2020) 9:328–41. doi: 10.1002/sctm.19-0173
- Trainor PA. Specification of neural crest cell formation and migration in mouse embryos. *Semin Cell Dev Biol.* (2005) 16:683–93. doi: 10.1016/j.semcdb.2005.06.007
- Srivastava D, Thomas T, Lin Q, Kirby ML, Brown D, Olson EN. Regulation of cardiac mesodermal and neural crest development by the bHLH transcription factor, dHAND. *Nat Genet.* (1997) 16:154–60. doi: 10.1038/ng0697-154
- Yanagisawa H, Clouthier DE, Richardson JA, Charité J, Olson EN. Targeted deletion of a branchial arch-specific enhancer reveals a role of dHAND in craniofacial development. *Development.* (2003) 130:1069–78. doi: 10.1242/dev.00337
- Howard MJ, Stanke M, Schneider C, Wu X, Rohrer H. The transcription factor dHAND is a downstream effector of BMPs in sympathetic neuron specification. *Development.* (2000) 127:4073–81. doi: 10.1242/dev.127.18.4073
- He F, Hu X, Xiong W, Li L, Lin L, Shen B, et al. Directed Bmp4 expression in neural crest cells generates a genetic model for the rare human bony synnathia birth defect. *Dev Biol.* (2014) 391:170–81. doi: 10.1016/j.ydbio.2014.04.013
- Stottmann RW, Anderson RM, Klingensmith J. The BMP antagonists Chordin and Noggin have essential but redundant roles in mouse mandibular outgrowth. *Dev Biol.* (2001) 240:457–73. doi: 10.1006/dbio.2001.0479
- Funato N, Kokubo H, Nakamura M, Yanagisawa H, Saga Y. Specification of jaw identity by the Hand2 transcription factor. *Sci Rep.* (2016) 6. doi: 10.1038/srep28405
- Funato N, Chapman SL, McKee MD, Funato H, Morris JA, Shelton JM, et al. Hand2 controls osteoblast differentiation in the branchial arch by inhibiting DNA binding of Runx2. *Development.* (2009) 136:615–25. doi: 10.1242/dev.029355
- Alexander T, Nolte C, Krumlauf R. Hox genes and segmentation of the hindbrain and axial skeleton. *Annu Rev Cell Dev Biol.* (2009) 25:431–56. doi: 10.1146/annurev.cellbio.042308.113423
- Couly G, Grapin-Botton A, Coltey P, Ruhin B, Le Douarin NM. Determination of the identity of the derivatives of the cephalic neural crest: incompatibility between Hox gene expression and lower jaw development. *Development.* (1998) 125:3445–59. doi: 10.1242/dev.125.17.3445
- Hunter MP, Prince VE. Zebrafish hox paralogue group 2 genes function redundantly as selector genes to pattern the second pharyngeal arch. *Dev Biol.* (2002) 247:367–89. doi: 10.1006/dbio.2002.0701
- Gendron-Maguire M, Mallo M, Zhang M, Gridley T. Hoxa-2 mutant mice exhibit homeotic transformation of skeletal elements derived from cranial neural crest. *Cell.* (1993) 75:1317–31. doi: 10.1016/0092-8674(93)90619-2
- Rijli FM, Mark M, Lakkaraju S, Dierich A, Dollé P, Chambon P. A homeotic transformation is generated in the rostral branchial region of the head by disruption of Hoxa-2, which acts as a selector gene. *Cell.* (1993) 75:1333–49. doi: 10.1016/0092-8674(93)90620-6
- Si N, Meng X, Lu X, Zhao X, Li C, Yang M, et al. Identification of loss-of-function HOXA2 mutations in Chinese families with dominant bilateral microtia. *Gene.* (2020) 757:144945. doi: 10.1016/j.gene.2020.144945
- Rosin JM, Li W, Cox LL, Rolfe SM, Latorre V, Akiyama JA, et al. A distal 594 bp ECR specifies Hmx1 expression in pinna and lateral facial morphogenesis and is regulated by the Hox-Pbx-Meis complex. *Development.* (2016) 143:2582–92. doi: 10.1242/dev.133736
- Di Bonito M, Narita Y, Avallone B, Sequino L, Mancuso M, Andolfi G, et al. Assembly of the auditory circuitry by a Hox genetic network in the mouse brainstem. *PLoS Genet.* (2013) 9:e1003249. doi: 10.1371/journal.pgen.1003249
- Vieux-Rochas M, Mascrez B, Krumlauf R, Duboule D. Combined function of HoxA and HoxB clusters in neural crest cells. *Dev Biol.* (2013) 382:293–301. doi: 10.1016/j.ydbio.2013.06.027